Solving the Helmholtz equation for membranes of arbitrary shape: numerical results

2008 J. Phys. A: Math. Theor. 41 265206

(http://iopscience.iop.org/1751-8121/41/26/265206)

IOP PUBLISHING JOURNAL OF PHYSICS A: MATHEMATICAL AND THEORETICAL

J. Phys. A: Math. Theor. **41** (2008) 265206 (29pp) doi:10.1088/1751-8113/41/26/265206

Solving the Helmholtz equation for membranes of arbitrary shape: numerical results

Paolo Amore

Facultad de Ciencias CUICBAS, Universidad de Colima, Bernal Díaz del Castillo 340, Colima, Colima, Mexico
and
Physics Department, University of Texas at El Paso, El Paso, TX, USA

E-mail: paolo.amore@gmail.google.com

Received 27 January 2008, in final form 11 May 2008
Published 12 June 2008
Online at stacks.iop.org/JPhysA/41/265206

Abstract

I calculate the modes of vibration of membranes of arbitrary shape using a collocation approach based on little sinc functions. The matrix representation of the PDE obtained using this method is explicit and does not require the calculation of integrals. To illustrate the virtues of this approach, I have considered a large number of examples, part of them are taken from the literature, and part of them new. When possible, I have tested the accuracy of these results by comparing them with the exact results (when available) or with results from the literature. In particular, in the case of the L-shaped membrane, the first example discussed in the paper, I show that it is possible to extrapolate the results obtained with different grid sizes to obtain highly precise results. Finally, I also show that the present collocation technique can be easily combined with conformal mapping to provide numerical approximations to the energies which quite rapidly converge to the exact results.

PACS numbers: 03.30.+p, 03.65.−w

(Some figures in this article are in colour only in the electronic version)

1. Introduction

This paper considers the problem of solving the Helmholtz equation

$$-\Delta\psi(x, y) = E\psi(x, y) \tag{1}$$

over a two-dimensional domain, B, of arbitrary shape, assuming Dirichlet boundary conditions over the border, ∂B. Physically, this equation describes the classical vibration of a homogeneous membrane or the behaviour of a particle confined in a region with infinite walls in quantum mechanics. Unfortunately exact solutions to this equation are available only

in few cases, such as for a rectangular or a circular membrane, where they can be expressed in terms of trigonometric and Bessel functions, respectively [1]. In the majority of cases, in fact, only numerical approaches can be used: some of these approaches are discussed, for example, in a beautiful paper by Kuttler and Sigillito [2]. The purpose of the present paper is to introduce a different approach to the numerical solution of the Helmholtz equation (both homogeneous and inhomogeneous) and illustrate its strength and flexibility by applying it to a large number of examples.

The paper is organized as follows: in section 2, I describe the method and discuss its application to the classical problem of a L-shaped membrane; in section 3, I consider an homogeneous membrane, with the shape of Africa and calculate few states; in section 4, I consider two inequivalent membranes, which are known to be isospectral, obtaining a numerical indication of isospectrality; in section 5, I study an example of irregular drum; in section 6, the method is applied to study the emergence of bound states in a configuration of wires of negligible transverse dimension, in the presence of crossings; in section 7, I show that even more precise results can be achieved by combining the collocation method with a conformal mapping of the boundary. Finally, in section 8, I draw my conclusions.

2. The method

The method that I propose in this paper uses a particular set of functions, the *little sinc functions* (LSF) of [13, 14], to obtain a discretization of a finite region of the two-dimensional plane. These functions have been used with success in the numerical solution of the Schrödinger equation in one dimension, both for problems restricted to finite intervals and for problems on the real line. In particular, it has been proved that exponential convergence to the exact solution can be reached when variational considerations are made (see [13, 14]).

Although [13] contains a detailed discussion of the LSF, I will briefly review here the main properties, which will be useful in the paper. Throughout the paper, I will follow the notation of [13].

A little sinc function is obtained as an approximate representation of the Dirac delta function in terms of the wavefunctions of a particle in a box (being $2L$ the size of the box). Straightforward algebra leads to the expression

$$s_k(h, N, x) \equiv \frac{1}{2N}\left\{\frac{\sin((2N+1)\chi_-(x))}{\sin\chi_-(x)} - \frac{\cos((2N+1)\chi_+(x))}{\cos\chi_+(x)}\right\}, \tag{2}$$

where $\chi_\pm(x) \equiv \frac{\pi}{2Nh}(x \pm kh)$. An alternative expression for these functions in terms of Chebyshev polynomials reads [14]

$$s_k(h, N, x) \equiv \frac{1}{2N}\{U_{2N}[\cos\chi_-(x)] - U_{2N}[\sin\chi_+(x)]\}. \tag{3}$$

The index k takes the integer values between $-N/2+1$ and $N/2-1$ (N being an even integer). The LSF corresponding to a specific value of k is peaked at $x_k = 2Lk/N = kh$, h being the grid spacing and $2L$ the total extension of the interval where the function is defined. By direct inspection of equation (2) it is found that $s_k(h, N, x_j) = \delta_{kj}$, showing that the LSF takes its maximum value at the kth grid point and vanishes on the remaining points of the grid.

It can be easily proved that the different LSF corresponding to the same set are orthogonal [13]:

$$\int_{-L}^{L} s_k(h, N, x)s_j(h, N, x)\,\mathrm{d}x = h\delta_{kj} \tag{4}$$

and that a function defined on $x \in (-L, L)$ may be approximated as

$$f(x) \approx \sum_{k=-N/2+1}^{N/2-1} f(x_k) s_k(h, N, x). \tag{5}$$

This formula can be applied to obtain a representation of the derivative of a LSF in terms of the set of LSF as

$$\begin{aligned} \frac{\mathrm{d}s_k(h, N, x)}{\mathrm{d}x} &\approx \sum_j \left.\frac{\mathrm{d}s_k(h, N, x)}{\mathrm{d}x}\right|_{x=x_j} s_j(h, N, x) \equiv \sum_j c_{kj}^{(1)} s_j(h, N, x), \\ \frac{\mathrm{d}^2 s_k(h, N, x)}{\mathrm{d}x^2} &\approx \sum_j \left.\frac{\mathrm{d}^2 s_k(h, N, x)}{\mathrm{d}x^2}\right|_{x=x_j} s_j(h, N, x) \equiv \sum_j c_{kj}^{(2)} s_j(h, N, x), \end{aligned} \tag{6}$$

where the expressions for the coefficients $c_{kj}^{(r)}$ can be found in [13]. Although equation (5) is approximate and the LSF strictly speaking do not form a basis, the error made with this approximation decreases with N and tends to zero as N tends to infinity, as shown in [13]. For this reason, the effect of this approximation is essentially to replace the continuum of an interval of size $2L$ on the real line with a discrete set of $N-1$ points, x_k, uniformly spaced on this interval.

Clearly these relations are easily generalized to functions of two or more variables. Since the focus of this paper is on two-dimensional membranes, I will briefly discuss how the LSF are used to discretize a region of the plane; the extension to higher dimensional spaces is straightforward. A function of two variables can be approximated in terms of $(N_x - 1) \times (N_y - 1)$ functions, corresponding to the direct product of the $N_x - 1$ and $N_y - 1$ LSF in the x- and y-axis: each term in this set corresponds to a specific point on a rectangular grid with spacings h_x and h_y (in this paper, I use a square grid with $N_x = N_y = N$ and $L_x = L_y = L$).

Since (k, k') identifies a unique point on the grid, I can select this point using a single index

$$K \equiv k' + \frac{N}{2} + (N-1)\left(k + \frac{N}{2} - 1\right) \tag{7}$$

which can take the values $1 \leqslant K \leqslant (N-1)^2$. I can also invert this relation and write

$$k = 1 - N/2 + \left[\frac{K}{N - 1 + \varepsilon}\right], \tag{8}$$

$$k' = K - N/2 - (N-1)\left[\frac{K}{N - 1 + \varepsilon}\right], \tag{9}$$

where $[a]$ is the integer part of a real number a and $\varepsilon \to 0$.

As a natural extension of the results presented in [13, 14], I can consider the Schrödinger equation in two dimensions

$$\hat{H}\psi_n(x, y) \equiv [-\Delta + V(x, y)]\psi_n(x, y) = E_n \psi_n(x, y) \tag{10}$$

using the convention of assuming a particle of mass $m = 1/2$ and setting $\hbar = 1$. The Helmholtz equation, which describes the vibration of a membrane, is a special case of (10), corresponding to having $V(x, y) = 0$ inside the region $\mathcal{B}$ where the membrane lies and $V(x, y) = \infty$ on the border $\partial\mathcal{B}$ and outside the membrane.

The discretization of equation (10) proceeds in a simple way using the properties discussed in equations (5) and (6):

$$H_{kk',jj'} = -\left[c_{kj}^{(2)} \delta_{k'j'} + \delta_{kj} c_{k'j'}^{(2)}\right] + \delta_{kj}\delta_{k'j'} V(x_k, y_{k'}), \tag{11}$$

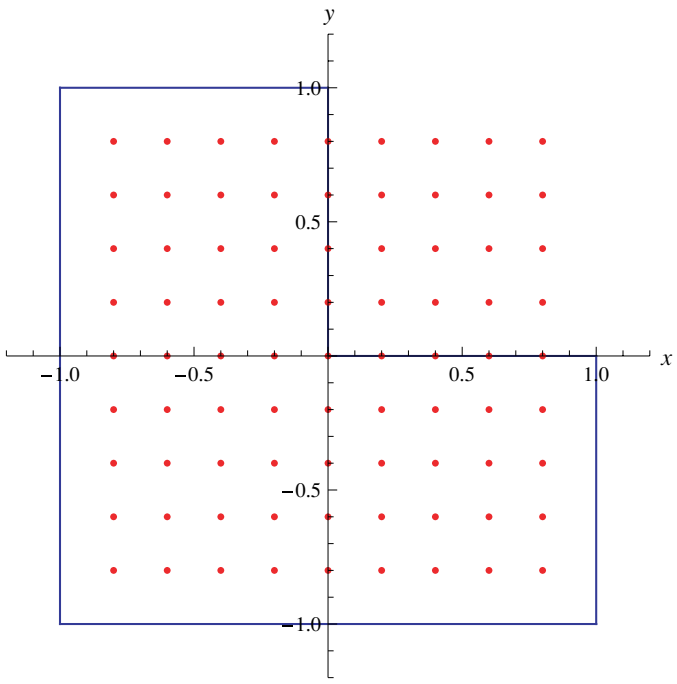

Figure 1. L-shaped membrane. The dots are the collocation points corresponding to $N = 10$.

where k, j, k', j' take the values $-N/2+1, \ldots, N/2-1$. Note that the potential part of the Hamiltonian is obtained by simply 'collocating' the potential $V(x, y)$ on the grid, an operation with a limited computational price. The result shown in (11) corresponds to the matrix element of the Hamiltonian operator $\hat{H}$ between two grid points, (k, k') and (j, j'), which can be selected using two integer values K and J, as shown in (7).

Following this procedure, the solution of the Schrödinger (Helmholtz) equation on the uniform grid generated by the LSF corresponds to the diagonalization of a $(N-1)^2 \times (N-1)^2$ square matrix, whose elements are given by equation (11).

I will now use a specific problem, the vibration of a L-shaped membrane, represented in figure 1, to illustrate the method, and discuss different implementations of the method itself. This problem has been widely used in the past to test the performance of the different numerical methods (see, for example [2–5, 7–11]) and is therefore a useful tool to assess the strength of the present approach. Because of the reentrant corner, corresponding to the angle $\theta = 3\pi/2$ located at $(0, 0)$, the derivatives of $\psi(x, y)$ in the radial direction are unbounded (see [3]).

Reid and Walsh [3] obtained a numerical approximation for the two lowest modes of this membrane using finite differences and a conformal map which eliminates the reentrant corner (see figure 5 of [3]); a more precise result was later obtained by Fox, Henrici and Moler who used the method of particular solutions (MPS) in [4] exploiting the symmetries of the problem (the reader may find a detailed discussion of the symmetries for this problem in [2]): the first eight digits of the lowest eigenvalue reported by the authors are correct. Mason has obtained numerical estimates for the first few modes of the L-shaped membrane in terms of a two-dimensional Chebyshev series [5]. Milsted and Hutchinson [6] have obtained finite element

solutions to this problem. Sideridis [7] used a conformal mapping of the L-shaped region onto a square and then solved the resulting equation on a uniform rectangular mesh, obtaining the first four digits of the lowest mode. Schiff [8] has calculated the first 15 lowest modes of this membrane using finite elements, with a refined grid covering the region surrounding the reentrant corner.

More recently, Platte and Driscoll have solved the boundary value problem on the L-shaped membrane using radial basis functions [9]. Finally, Betcke and Trefethen have revisited the MPS in [10]; in that paper, they have observed that the MPS reaches a minimal error for a certain value of N (the number of collocation points on each of the sides non-adjacent to the corner where the expansion is performed) but then it starts to grow as N increases. The modified version of the method discussed in [10], which samples the Fourier–Bessel functions also in the interior points, corrects this problem and provides a convergent behaviour for the error. In this way, Betcke and Trefethen were able to obtain the first 14 digits of the lowest eigenvalue of the L-shaped membrane, $E_1 \approx 9.639\,723\,844\,0219$. I will use this precise result to test the accuracy of our method. Reference [11] contains precise estimates for some higher excited states of the L-shaped membrane.

I will now apply the LSF to the numerical solution of this problem: looking at figure 1, I consider the grid points which are internal to the membrane and which do not fall on the border. For a fixed N there is a total of $3/4N^2 - 2N + 1$ points; the grid represented in the figure corresponds to $N = 10$ and therefore to a total of 56 internal points. In this case the collocation of the Hamiltonian on the uniform grid generated by the LSF leads to a 56×56 matrix, which can then be diagonalized. The eigenvalues of this matrix provide the lowest 56 modes of the membrane, while the eigenvectors provide the lowest 56 wavefunctions. Alternatively I can pick all the points of the grid internal to the membrane, including those falling on the border: in such a case a total of $3/4N^2 - N$ points are found, corresponding to a total of 65 points in the case of the figure.

Table 1 contains the first 108 eigenvalues of the L-shaped membrane calculated using a grid with $N = 60$ and selecting the grid points according to the prescriptions just explained. I have used the notation $E_n^{(\pm)}$ for the energy of the nth state when the collocation points on the border are either rejected $\left(E_n^{(+)}\right)$ or kept $\left(E_n^{(-)}\right)$. The notation $(\pm)$ is used since the two sets approach the exact results either from above $(+)$ or from below $(-)$, as one can see comparing these numbers with the precise results contained in [10, 11]. The reader will certainly note that the results of table 1 contain rather large errors: in the case of the fundamental state, for example, one has an error of about 1% from $E_n^{(+)}$ and a much larger error of almost 5% for $E_n^{(-)}$.

The left panel of figure 2 shows the eigenvalues $E_n^{(+)}$ (solid line) and $E_n^{(-)}$ (dashed line) for the L-shaped membrane corresponding to a grid with $N = 60$. The reader may note that the higher end of the spectrum displays a curvature, contrary to the behaviour predicted by Weyl's law, i.e. $\langle N \rangle \propto E$ for large energies. It is easy to show that such effect is artificial: consider, for example, the case of a particle confined in a unit square, whose energies are given by $E_{n_x,n_y} = \left(n_x^2 + n_y^2\right)\pi^2$. The diagonalization of the Hamiltonian (11) for this problem would provide the energies corresponding to the $(N-1)^2$ states obtained taking the first $N-1$ values of n_x and n_y. This means that for energies higher than $E_N = [N^2 - 2N + 2]\pi^2$ the method will provide only the eigenvalues contained inside a square of side $N - 1$ (in the (n_x, n_y) plane), up to a maximal energy $E_{\mathrm{MAX}} = 2[N^2 - 2N + 2]\pi^2$. For this reason, the states above E_N are incomplete and should not be taken into account for inferring the asymptotic behaviour of $\langle N \rangle$. The right panel of figure 2 displays the asymmetry defined as $\mathcal{A}_n = 2\left(E_n^{(+)} - E_n^{(-)}\right)/\left(E_n^{(+)} + E_n^{(-)}\right)$ for the same grid: this quantity provides an upper estimate for the error.

Table 1. First 108 eigenvalues of the L-shaped membrane calculated with a grid with $N = 60$.

n	$E_n^{(-)}$	$E_n^{(+)}$	n	$E_n^{(-)}$	$E_n^{(+)}$	n	$E_n^{(-)}$	$E_n^{(+)}$
1	9.177164983	9.725740015	37	178.4844965	184.8421046	73	343.7275747	361.2225873
2	14.78073926	15.25792488	38	193.8672234	197.9262249	74	344.9934435	361.9427155
3	19.37069304	19.79218759	39	193.8814147	197.9267047	75	358.2837562	366.3264978
4	29.22316338	29.5638567	40	198.1817051	201.9430968	76	359.5348189	366.3670805
5	30.96354609	32.09126661	41	201.4624222	208.1352708	77	364.75956	370.6707929
6	40.02046425	41.71342235	42	208.0809373	208.8812769	78	365.5537093	373.5349023
7	43.35567534	45.16667725	43	208.3091478	209.9202486	79	367.4408345	377.7859531
8	48.49170563	49.48205954	44	218.9529607	223.795143	80	371.1572423	384.5448247
9	48.50129154	49.48210584	45	219.7977882	224.2020086	81	380.3860374	390.8564172
10	55.00253452	56.99285853	46	230.4881589	237.0180886	82	381.619838	391.5359069
11	64.39311656	65.51743185	47	234.522406	238.9225242	83	389.8803312	395.9403897
12	70.17580289	71.22539692	48	240.8305192	247.399449	84	390.1339997	395.9528626
13	70.75536576	71.694315	49	241.3085263	247.4007186	85	396.7580769	405.7350508
14	77.43821507	79.16827278	50	242.091938	251.9722965	86	396.783386	405.7417585
15	85.62358216	89.95280767	51	242.4936924	253.9585512	87	405.4299759	417.4274921
16	89.20133569	92.66479784	52	252.6896353	257.3835642	88	409.020823	421.0196083
17	95.02656477	97.67618899	53	254.3713602	257.4891189	89	422.9007962	426.9812301
18	96.44902117	98.9581845	54	258.45965	267.2165568	90	425.5099017	427.4264825
19	97.50939511	98.98841467	55	262.2523481	270.362378	91	425.6809979	434.295792
20	99.15370293	102.1148968	56	262.9019839	271.2576246	92	435.8786896	444.6206086
21	109.8094028	112.7440906	57	276.4727322	282.0671402	93	435.9192729	445.3287181
22	112.6706295	115.940658	58	279.3270569	286.9614486	94	438.0162243	445.3290091
23	125.8637839	128.647868	59	281.7073779	287.0144046	95	442.0953758	454.6858173
24	126.0084139	128.6517412	60	284.1271564	290.2236089	96	449.9029921	454.7270884
25	129.4077703	130.2193886	61	287.835501	294.4411423	97	450.2786574	456.2838516
26	129.4610293	130.4087363	62	301.6031656	306.989597	98	455.431713	465.7654543
27	138.4732345	143.0937626	63	304.0018517	307.2227265	99	463.9179935	480.155258
28	148.8908462	151.4047394	64	307.1623397	311.2775619	100	464.4999312	481.0156905
29	149.3132131	155.4149531	65	308.637254	314.7477734	101	468.8725774	488.2586507
30	157.1294641	162.6916706	66	310.2539585	316.6847591	102	471.7598792	491.8389757
31	159.2280728	165.3935921	67	328.509336	336.1784596	103	478.7708593	494.7920322
32	159.647457	165.4142765	68	328.7797637	336.2277068	104	484.8647328	494.949551
33	166.1106112	168.2997856	69	330.9763129	336.5300454	105	485.0320322	495.6089426
34	166.1907708	168.3155339	70	332.6951225	336.5831701	106	493.2198808	501.7272125
35	173.3430437	178.1220953	71	340.1437751	346.949885	107	493.4054114	503.8197404
36	175.4511857	180.5827508	72	340.2548393	353.4120482	108	499.6245389	514.1288667

Figure 3 displays the ground-state energy of the L-shaped membrane as a function of the number of grid points and compares it with the precise result of [10]: as already pointed out the two sets approach the exact value from above and below.

Much more precise results can be obtained by performing an extrapolation of the results corresponding to finite grids: this is a common procedure used in the literature (see, for example [2]). I have considered four different extrapolation sets using the numerical results obtained working with grids with N ranging from $N = 10$ to $N = 60$ (only even values). Calling $h = 2L/N$ the grid spacing the sets are

$$f_1(h) = \sum_{n=0}^{\bar{N}} c_n h^n, \tag{12}$$

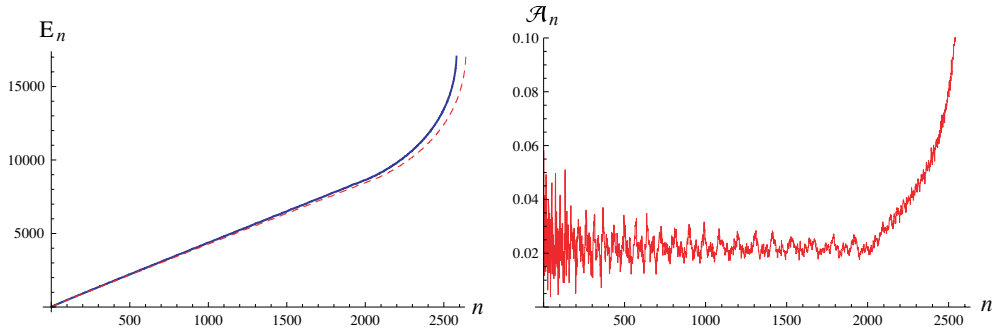

Figure 2. Left panel: Energy of the ground state of the L-shaped membrane as a function of the number of grid points N. The horizontal line is the precise result of [10]. The set approaching the exact result from above (below) corresponds to $E_1^{(+)}$ ($E_1^{(-)}$). Right panel: The asymmetry $\mathcal{A}_n = 2(E_n^{(+)} - E_n^{(-)})/(E_n^{(+)} + E_n^{(-)})$ calculated with a grid with $N = 60$.

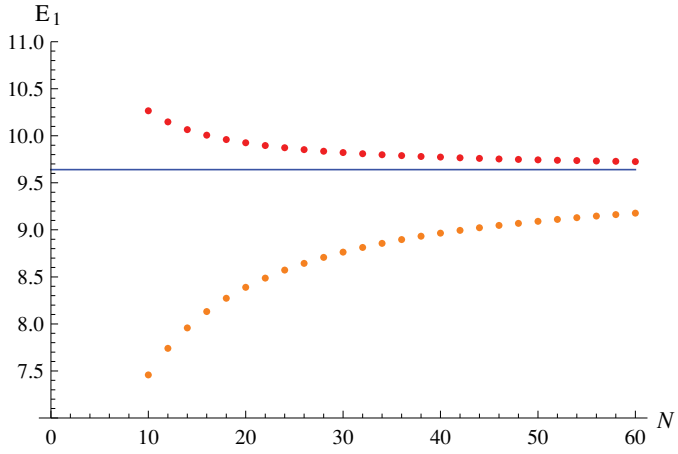

Figure 3. Energy of the ground state of the L-shaped membrane as a function of the number of grid points N. The horizontal line is the precise result of [10]. The set approaching the exact result from above (below) corresponds to $E_1^{(+)}$ ($E_1^{(-)}$).

$$f_2(h) = \frac{\sum_{n=0}^{\bar{N}/2} c_n h^n}{1 + \sum_{n=1}^{\bar{N}/2} c_n h^n}, \tag{13}$$

$$f_3(h) = c_0 + \sum_{n=1}^{\bar{N}} c_n h^{n/3+2/3}, \tag{14}$$

$$f_4(h) = \frac{c_0 + \sum_{n=1}^{\bar{N}/2} c_n h^{n/3+2/3}}{1 + \sum_{n=1}^{\bar{N}/2} c_n h^{n/3+2/3}}, \tag{15}$$

where $\bar{N}$ is an even integer which determines the number of coefficients used in the fits.

The continuum limit is reached taking $h \to \infty$, where only the coefficient c_0 survives. The unknown coefficients in expressions (12)–(15) are obtained using a least square approach:

Table 2. Extrapolation of selected eigenvalues of the L-shaped membrane using the four different sets. The first six states correspond to extrapolating the results for grids going from $N = 10$ to $N = 60$, with 25 unknown coefficients; the last two states correspond to extrapolating the results for grids going from $N = 18$ to $N = 60$, and with 21 unknown coefficients. For a given state, the set with the asterisk corresponds to the minimal value taken by the least squares. The results which do not converge to the exact value have been omitted.

n		Set 1	Set 2	Set 3	Set 4
1	(−)	9.63959383529194	9.63970774930113	9.63972385784876	9.63972384404696*
1	(+)	9.63959513453456	9.63971258279395	9.63972384034031	9.63972384401891*
2	(−)	15.1972518419212	15.1974702475024	15.1972519362081	15.1972519266011*
2	(+)	15.1972518428845	15.1972519235114	15.1972519387503	15.1972519264561*
3	(−)	19.7392087861784	19.7392088017282	19.7392073765870	19.7392088020095*
3	(+)	19.7392088019879	19.7392088021704	19.7392087962239	19.7392088021785*
4	(−)	29.5178267971821	29.5214811097206	–	29.5214811103487*
4	(+)	29.5214810813053	29.5214811126514	29.5214794563921	29.5214811141506*
5	(−)	31.9159767579531	31.9125745966885	–	31.9126359533035*
5	(+)	31.9123209946513	31.9126005580344	31.9126386707453	31.9126359571263*
6	(−)	41.474267306813	41.4744740922213	41.4761914432832	41.4745099148779*
6	(+)	41.4742739974452	41.4744780007070	41.4741677038785	41.4745098904487*
20	(−)	101.776561675314*	101.605333389975	–	99.7713224851033
20	(+)	101.604853531780	101.605223692426	101.673183488214	101.605294080845*
50	(−)	–	246.740564791939	–	246.602432808866*
50	(+)	250.784799377301	250.785244396338	–	250.785494606618*
104	(−)	–	410.08260648211	–	–
104	(+)	493.480067984180*	493.480206216096	–	493.488405725447

I show the results of this procedure in table 2. In general, the last set provides the best results and indeed reproduces the first 11 digits of E_1 correctly, using either the values of $E_1^{(-)}$ or those of $E_1^{(+)}$. In the case of E_3, for which the exact value is known ($E_3 = 2\pi^2$), I obtain the first 14 digits correct using $E_3^{(+)}$ and the first 11 digits correct using $E_3^{(-)}$.

In [15] Berry has devised an algorithm for obtaining successive approximations to the geometric properties K_j of a closed boundary B given the lowest N eigenvalues E_n. The partition function $\Phi(t) \equiv \sum_{n=1}^{\infty} \mathrm{e}^{-E_n t}$ obeys an asymptotic expansion for small values of t

$$\Phi(t) \approx \frac{1}{t} \sum_{j=0}^{\infty} K_j t^{j/2}, \tag{16}$$

where the coefficients K_j are related to the geometric properties of B. For example, $K_0 = A/4\pi$ and $K_1 = -\gamma L/8\sqrt{\pi}$. Using this asymptotic expansion, Berry has obtained accelerated expressions for the geometrical constants of B. In particular, for the area of B he has found the approximant (equation (20) of [15])

$$A_m(t) = \frac{2\pi t}{m!} \sum_{n=1}^{\infty} \mathrm{e}^{-\xi_n^2} \xi_n^{m-1} H_{m+1}(\xi_n), \tag{17}$$

where $\xi_n \equiv \sqrt{E_n t}$.

In the left panel of figure 4 I show the area approximant $A_2(t)$, obtained using the expression of Berry. The thin lines correspond to using the sets $E_n^{(+)}$ and $E_n^{(-)}$ (solid and dashed lines, respectively); the thick lines correspond to using the eigenvalues obtained from the extrapolation of the sets $E_n^{(+)}$ and $E_n^{(-)}$ (solid and dashed lines, respectively). I call $\bar{E}_n^{(\pm)}$ the eigenvalues obtained extrapolating the eigenvalues $E_n^{(\pm)}$; the extrapolation is carried out using

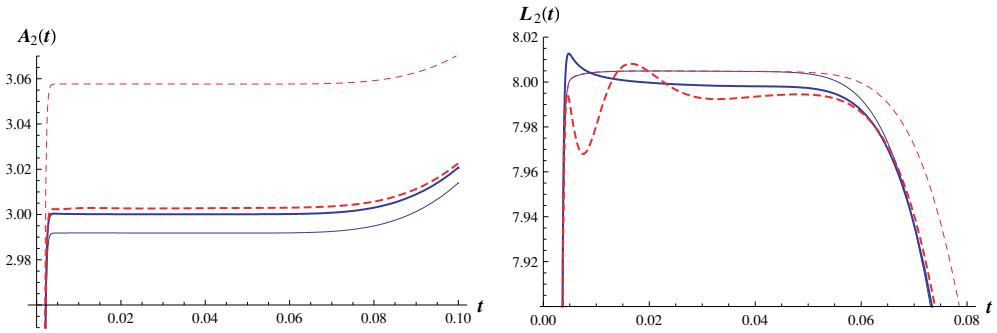

Figure 4. Left panel: The area approximant $A_2(t)$ obtained using the expression of Berry. The thin solid and dashed lines are obtained with the first 1000 eigenvalues corresponding to the sets $E_n^{(+)}$ and $E_n^{(-)}$, respectively. The bold solid and dashed lines correspond to the sets obtained through an extrapolation from the original sets. Right panel: The perimeter approximant $L_2(t)$ obtained with the improved expression of Berry. The same sets of eigenvalues have been considered.

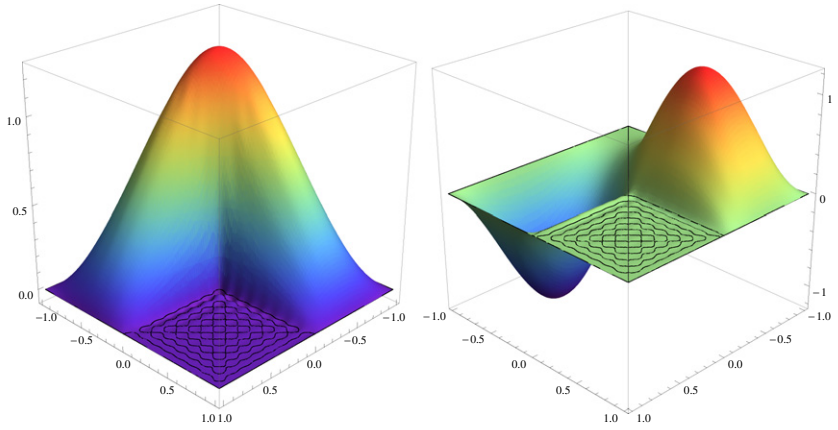

Figure 5. First two eigenfunctions of the L-shaped membrane obtained using $N = 30$. The black lines correspond to the level $\psi(x, y) = 0$.

the results obtained with grids with N going from 48 to 60 and assuming $E_n(N) \approx \bar{E}_n + \frac{\epsilon_n}{N}$. The approximants obtained with the extrapolated eigenvalues provide excellent approximations to the area and perimeter of the membrane, as seen in figure 4.

Figure 5 shows the first two eigenfunctions of the L-shaped membrane obtained with a grid corresponding to $N = 30$. The solid lines appearing in the 'forbidden region' correspond to the level $\psi(x, y) = 0$: the effect observed in the figure is due to the approximation of working with a finite number of grid points. In fact, although a particular LSF vanishes on the points defining the grid, except on a particular point, where it reaches its maximum, it is nonzero elsewhere. This means that the numerical solution can take small values even in the region where the exact solution must vanish; however, the size of this effect decreases as the number of grid points is increased (taking into account that the computational load roughly increases as N^4). In the appendix we propose an alternative procedure which does not involve the diagonalization of larger matrices and which can be used to improve the results obtained with a given grid.

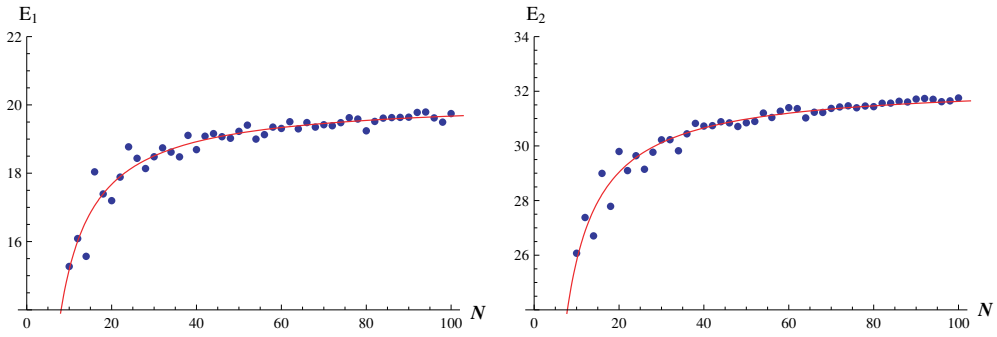

Figure 6. Left: energy of the fundamental mode of the Africa-shaped membrane as a function of the number of grid points. The continuous line is the fit $E_1 = a + b/N$, with $a = 20.1705$. Right: energy of the first excited mode of the Africa-shaped membrane as a function of the number of grid points. The continuous line is the fit $E_1 = a + b/N$, with $a = 32.2774$.

3. The Africa drum

I will now examine the case of a membrane with an irregular shape. The application of the method proceeds exactly as in the case of the L-shaped membrane: once a grid is chosen, the points of the grid which are internal to the membrane are used to build a matrix representation of the Hamiltonian which, once diagonalized, provides the energies and wavefunctions of the problem.

As a paradigm of this class of membranes, I have studied the vibrations of a drum with the shape of Africa[1]. Unlike in the previous example the border does not cross the grid points, a feature which affects the precision of the results. The plots in figure 6 display the energies of the first two states of the Africa drum for grids with different N (the dots in the plots) and compare them with the best fit obtained assuming that $E(N) = a + b/N$, where a and b are constants independent of N. The irregularity of the border is reflected in the behaviour of the eigenvalues which decay with N but at the same time oscillate.

In figure 7, I show the density plot of four different states of the Africa drum, obtained using a grid with $N = 60$. In figure 8, I show the wavefunction of the ground state of the Africa drum, obtained using a grid with $N = 60$.

4. Isospectral membranes

In a classic paper dated 1966 [16], Kac formulated an interesting question: whether it is possible to hear the shape of a drum, meaning if the spectrum of frequencies of a given drum is unique to that drum or drums with different shapes can have the same spectrum. The question was finally answered in 1992, when Gordon, Webb and Wolpert found a first example of inequivalent drums having the same spectrum [17]. An experiment made by Sridhar and Kudrolli reported in [18] used microwave cavities with the shape of the drums of [17] to verify the equality of the spectrum for the lowest 54 states. More recently, the same experiments have been carried out on isospectral cavities where the classical dynamics changes from pseudo-integrable to chaotic [19]. Numerical calculations of the first few modes

[1] As a technical remark, the shape of Africa—or of arbitrary membranes—is obtained in the Mathematica code by reading a digital image and then by generating a function inside a unit square, whose values at a given point are 0 and 1 depending if the point falls inside or outside the membrane.

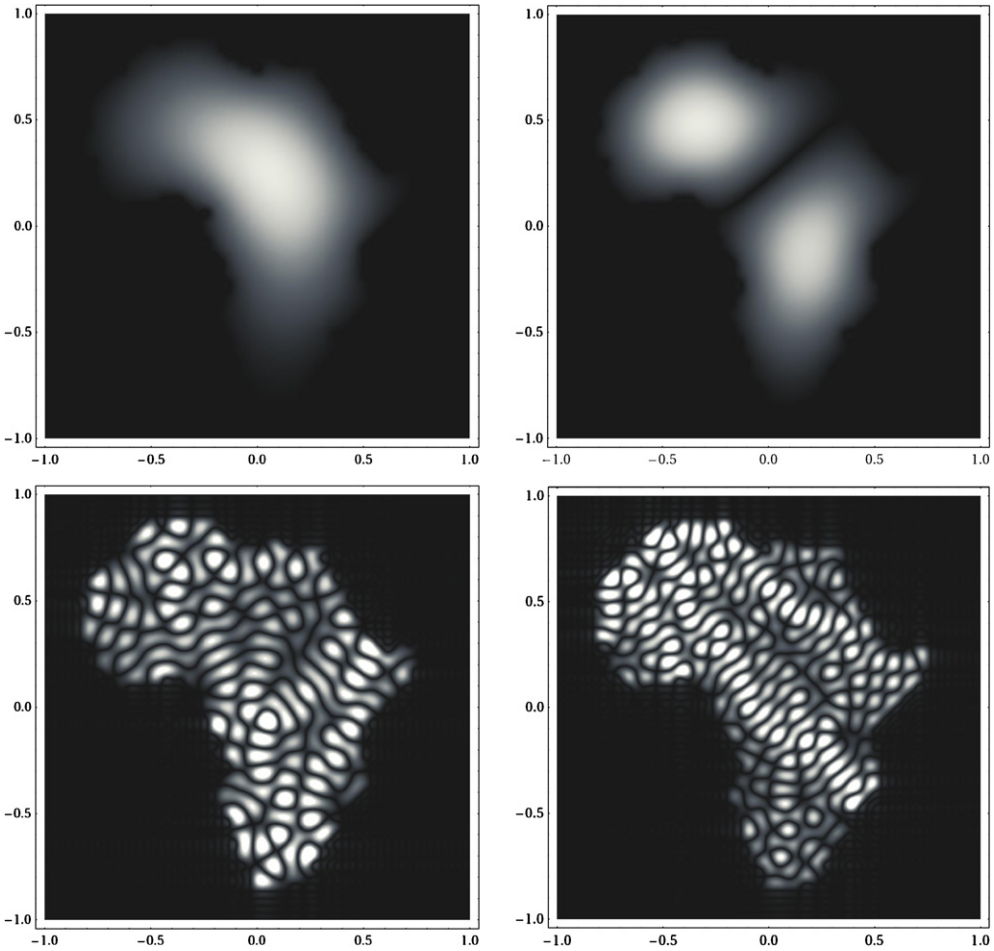

Figure 7. Density plot for the fundamental state (upper left), first excited state (upper right), 200th excited state (lower left) and 300th excited state (lower right) of the Africa-shaped membrane. In all plots the absolute value of the wavefunction is shown and a grid with $N = 60$ is used.

of the isospectral drums found in [17] have been performed with different techniques: Wu, Sprung and Martorell [20] have used a mode matching method to calculate the first 25 states of these drums and compared the results with those obtained with finite difference; using a different approach, Driscoll [21] has also calculated the first 25 states obtaining results which are accurate to 12 digits; Betcke and Trefethen [10] have used their modified version of the method of particular solutions to obtain the first three eigenvalues of these drums, reporting results which are slightly more precise than those of Driscoll.

I will now discuss the application of the present method to the calculation of the spectrum of these isospectral membranes: whereas in the case of the L-shaped membrane the border of the membrane was sampled by the grid, regardless of the grid size (keeping N even), in the case of the isospectral membranes this happens only for grids where $N = 6k$, with k an integer. It is important to restrict the calculation to this class of grids to avoid the oscillations observed

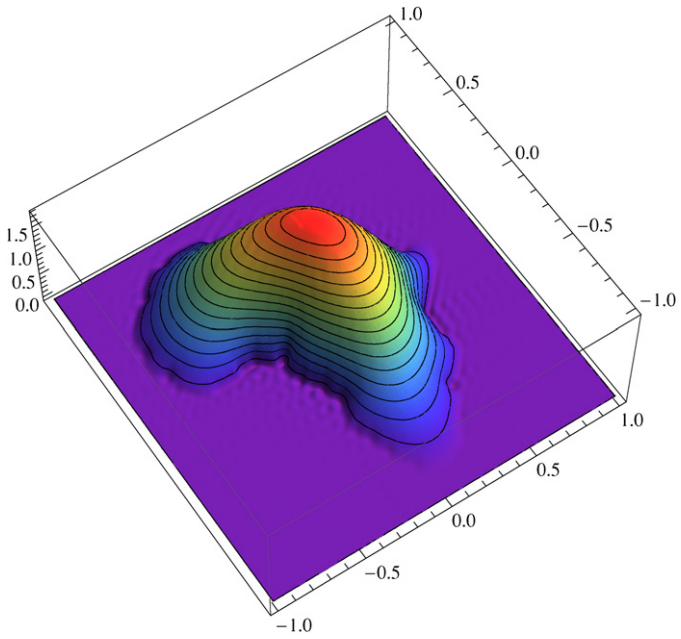

Figure 8. Ground state of the Africa-shaped membrane obtained using $N = 60$.

in the case of the Africa membrane. I have thus applied the method with grids ranging from $N = 6$ to $N = 120$.[2]

The plot in figure 9 displays the ground-state energy of the first isospectral membrane calculated at different grid sizes. The horizontal line is the precise value given in [10]. The set approaching this value from above (below) corresponds to the application of the method rejecting (accepting) the grid points falling on the border. The corresponding plot for the second isospectral membrane is almost identical and therefore it is not presented here.

In table 3, I report the energies of the first 30 states obtained using Richardson extrapolation [22] on the results for grids going from $N = 66$ to $N = 120$. The second and third columns are the energies of the first isospectral membranes obtained with the sets which reject $\left(E_n^{(+)}\right)$ or accept $\left(E_n^{(-)}\right)$ the grid points falling on the border, which as seen in the case of the L-shaped membrane provide a sequence of numerical values approaching the exact eigenvalue from above and from below, respectively. The last two columns report the analogous results for the second isospectral membrane. Note that some of the energies in the third column are clearly incorrect.

A further empirical verification of the isospectrality of the two membranes is presented in figure 10, where I have plotted the asymmetry $\mathcal{A}_n \equiv \left(E_n^{(1+)} - E_n^{(2+)}\right) \Big/ \left(E_n^{(1+)} + E_n^{(2+)}\right)$ for the first 2000 states of the isospectral membranes. In this case $E_n^{(1+)}$ $\left(E_n^{(2+)}\right)$ is the energy of the nth state of the first (second) membrane obtained using Richardson extrapolation of the grids with $N = 114$ and $N = 120$. Figure 11 displays the wavefunctions of the ground state and 100th state of the two isospectral membranes.

[2] The numerical results presented in the case of the L-shaped membrane were obtained with a 40-digit precision in the eigenvalues, using the command N[, 40] of Mathematica: in this case, since I need to resort to larger grids I have worked with less digits precision using the command $N[]$ in Mathematica.

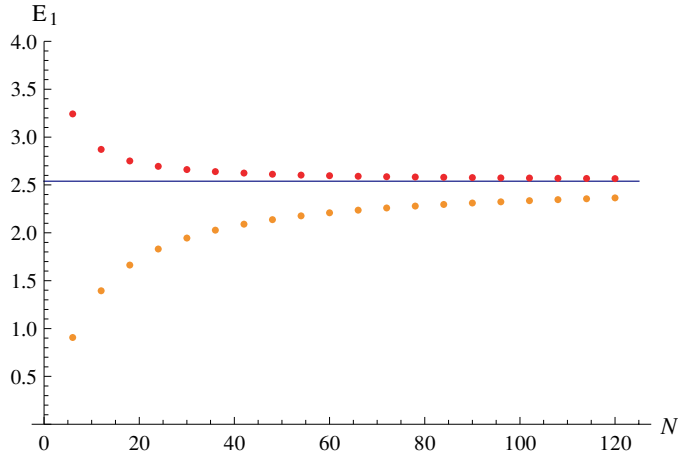

Figure 9. Energy of the ground state of the first isospectral membrane as a function of the number of grid points N. The horizontal line is the precise result of [10]. The set approaching the exact result from above (below) corresponds to $E_1^{(1+)}$ ($E_1^{(1-)}$).

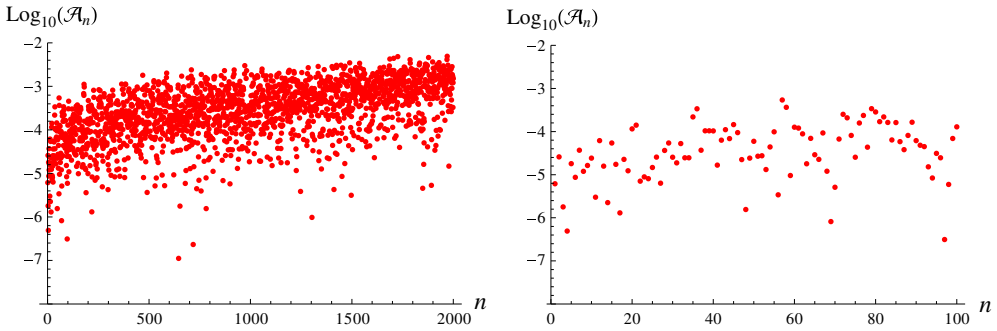

Figure 10. Left panel: $\log_{10}$ of the asymmetry $\mathcal{A}_n \equiv (E_n^{(1+)} - E_n^{(2+)})/(E_n^{(1+)} + E_n^{(2+)})$ for the first 2000 states of the isospectral membranes. $E_n^{(1+)}$ ($E_n^{(2+)}$) is the energy of the nth state of the first (second) membrane obtained using Richardson extrapolation of the grids with $N = 114$ and $N = 120$. Right panel: Blow-up of the previous plot for the first 100 states.

5. An unusual drum

I will now consider a further example by looking at a particular membrane originally studied by Trott [23]: this drum is shown in figure 12 and consists of a total of 308 units squares which are joined into a rather irregular form. Theoretical and experimental studies carried out on drums with fractal or irregular boundaries have shown that the wave excitations for these drums are drastically altered [24–26]: in particular, the Weyl law for these membranes is modified in a way which depends on the fractal dimension of the perimeter (see, for example [27]), the so-called Weyl–Berry–Lapidus conjecture. Recently, the vibrations of a uniform membrane contained in a Koch snowflake have been studied in two papers [28, 29].

The paper by Trott is both interesting in its physical and mathematical content and as an example of the excellent capabilities of Mathematica to handle heavy numerical calculations:

Table 3. First 30 eigenvalues of the isospectral membranes obtained with Richardson extrapolation of the results obtained with grids from $N = 66$ to $N = 120$.

n	$E_n^{(1+)}$	$E_n^{(1-)}$	$E_n^{(2+)}$	$E_n^{(2-)}$
1	2.537938184	2.537859157	2.537930157	2.537924672
2	3.655477379	3.655457482	3.655439267	3.655436933
3	5.175456364	5.175515223	5.1754891	5.175450085
4	6.53758046	6.537493542	6.537561774	6.537528448
5	7.247973684	7.248012453	7.247966062	7.248007219
6	9.209282216	9.209252596	9.20928929	9.209222008
7	10.59698943	10.59697476	10.59692509	10.59694683
8	11.54137149	11.54137651	11.54137016	11.54142735
9	12.33702671	12.33696554	12.33700655	12.33698898
10	13.05355072	13.0535318	13.05351736	13.05354013
11	14.31383084	14.31387457	14.31384362	14.31380888
12	15.87113023	15.87110476	15.87106608	15.8711794
13	16.94182893	-25414.06158	16.94177705	16.94177218
14	17.66507424	25448.66845	17.66503368	17.6650544
15	18.98079211	18.98079864	18.98083269	18.98081294
16	20.88240176	16.71191189	20.88233985	20.88246688
17	21.24773575	25.41816076	21.24772537	21.24764682
18	22.23265755	22.2326039	22.23265897	22.23262895
19	23.71129295	23.71135125	23.71127276	23.71130372
20	24.47925064	24.48080219	24.47920658	24.47934876
21	24.67406118	24.67245947	24.67401531	24.67403958
22	26.08011208	26.08090828	26.08008881	26.08012901
23	27.30391033	27.30298845	27.30390863	27.3039225
24	28.17508031	28.17506497	28.17506143	28.17505957
25	29.56976983	29.56970152	29.56975041	29.56905778
26	31.48308074	31.51241562	31.48304984	31.48393448
27	32.07624358	32.16454642	32.07622156	32.08008665
28	32.21611001	37.0118719	32.21605287	32.21393591
29	32.90535338	27.9888228	32.90537696	32.90354978
30	34.13633502	34.13929552	34.13632946	34.13632752

as a matter of fact Trott uses a finite difference approximation of the Laplacian on a uniform grid and samples the membrane in 28 521 internal points. Explicit numerical values for the first 24 modes are reported.

I have therefore considered the same problem using the LSF with grids of different size (up to $N = 250$ which leads to the same grid of [23]). Figure 13 displays the energy of the fundamental mode of this membrane as a function of the size of N. The dashed horizontal line in the plot represents the result of [23], $E_1 = 6.647\,05$: the points on the upper part of the plot correspond to N going from 50 to 250, with intervals of 50. For these particular values of N, the border of the membrane is sampled by the grid and therefore more accurate results are expected. The grid points on the border are rejected, which leads to eigenvalues which approach the exact results from above, as seen in the previous examples. The points in the lower part of the plot correspond to grid sizes varying from $N = 52$ to $N = 148$, excluding $N = 100$: in this case, the values approach the exact result from below, although in doing so they also oscillate reflecting the treatment of the border (a behaviour already observed in the case of the Africa membrane). As mentioned above, the finest grid corresponds to sampling the membrane on 28521 internal points and therefore to working with a

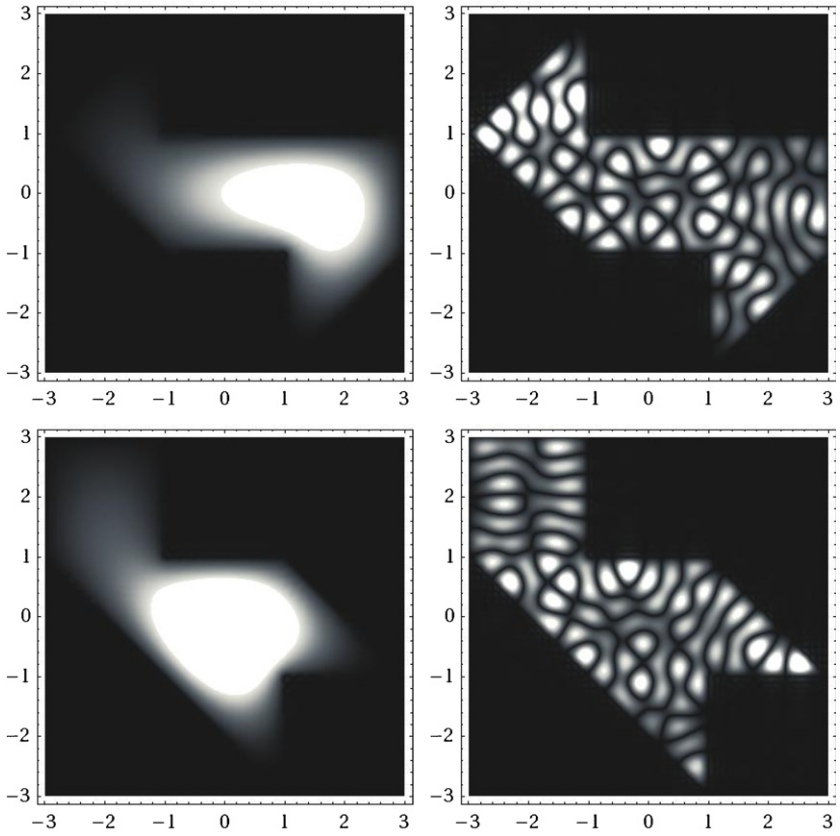

Figure 11. Upper panel: Wavefunctions (absolute value) of the first isospectral membrane (ground state and 100th excited state). Lower panel: Wavefunctions (absolute value) of the second isospectral membrane (ground state and 100th excited state). A grid with $N = 60$ is used.

28521×28521 square matrix. Given that the matrix obtained with the LSF is a sparse symmetrix matrix, it is possible to deal efficiently with it in Mathematica, applying the Arnoldi method to extract a limited sequence of eigenvalues/eigenvectors. The reader will note that in this example I have not considered the set corresponding to accepting the grid points falling on the border, as was done in the case of the L-shaped and of the isospectral membranes: although this set provides a sequence of values which uniformly approach the value at the continuum, the number of grid points sampled is quite large because of the large perimeter of the membrane. For example, for $N = 100$, this set samples the membrane on 7029 points, compared with the $N = 3801$ points used in the other set.

The figure also displays the improved ground-state energies obtained using the 'mesh refinement' procedure described in the appendix (the three green points): the eigenvector for a given grid is extrapolated to a finer grid rejecting contributions in the 'forbidden region' (i.e. falling outside the border of the membrane). The improved energy estimate corresponds to the expectation value of the Hamiltonian in this state and thus requires no diagonalization. The results displayed in the figure correspond to extrapolation to a grid which is twice finer.

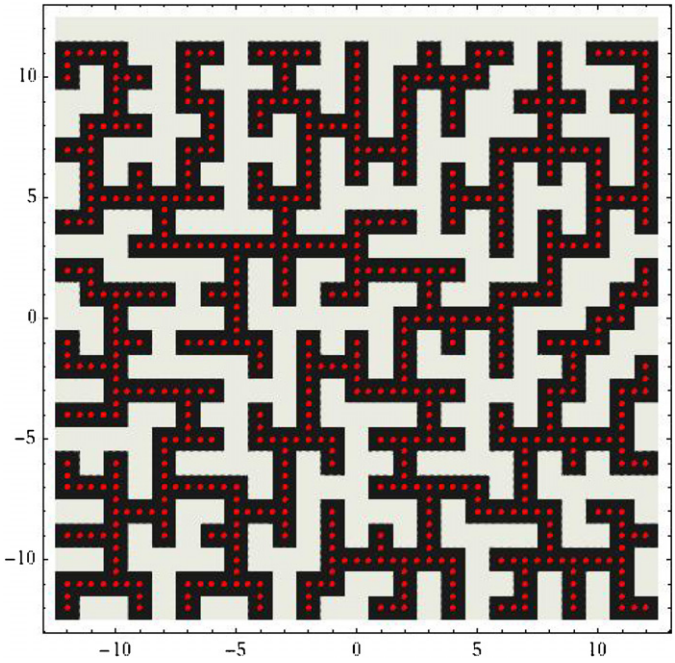

Figure 12. The unusual drum considered by Trott [23]. The black area is the surface of the drum; the red points are the collocation points corresponding to $N = 50$.

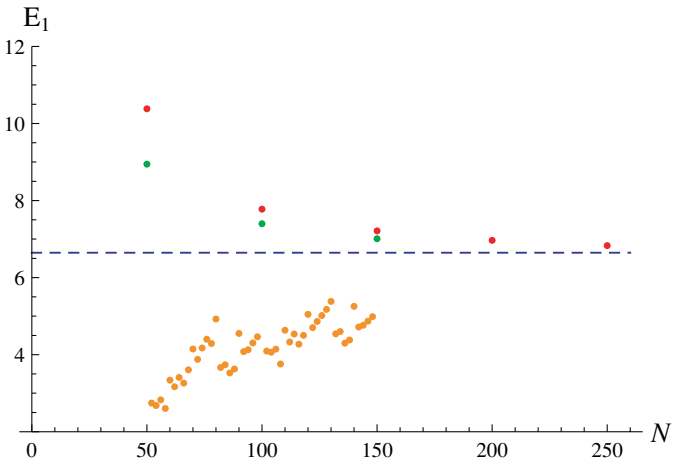

Figure 13. Energy of the ground state of the unusual drum as a function of N. The horizontal line is the result of [23]; the points approaching the horizontal line from above correspond to configurations where the border is sampled by the collocation points (and as discussed in the case of the L-shaped membrane are rejected). The green points correspond to the results obtained with the 'mesh refinement' procedure described in the appendix.

6. Bound states in the continuum

It is well known that the spectrum of the Laplacian with Dirichlet boundary conditions may contain bound states even for open geometries, in correspondence of crossings or bendings of

the domain. For example, Schult *et al* [30] have studied the problem of two crossed wires, of infinite length, showing that such a geometry supports exactly one bound state, localized at the crossing. Avishai and collaborators have also proved the existence of a bound state in the broken strip configuration for arbitrarily small angles, see [31] (more recently, Levin has proved the existence of one bound state in the broken strip for any angle of the strip [32]). Goldstone and Jaffe [33] have given a variational proof of the existence of a bound state for an infinite tube in two and three dimensions, provided that the tube is not straight. Other interesting configurations which support bound states in the continuum have been studied by Trefethen and Betcke [11].

The example which I will consider here is somehow related to the crossed wires configuration studied by Schult *et al*. I have considered a set of horizontal and vertical wires, of negligible transverse dimension, which are contained in a square box of size 2. Calling $\bar{n}$ the number of wires in each dimension, $\bar{n}^2$ is the number of crossings between these wires (for simplicity the wires are assumed to be equally spaced). This configuration can be easily studied in the present collocation approach, by sampling the wires on a grid and by then diagonalizing the Hamiltonian obtained following this procedure. The resulting energies calculated in this way will clearly depend on the spacing of the collocation grid, h, and diverge as h is sent to zero. To obtain finite results one need to multiply these eigenvalues by h^2, which eliminates the divergence caused by the shrinking of the transverse dimension. Following this procedure I have studied different configurations, corresponding to choosing different value of $\bar{n}$ (going from $\bar{n} = 1$ to $\bar{n} = 4$) and I have found that a given configuration has precisely the same number of bound states as the number of crossings. These bound states happen to be almost exactly degenerate and correspond to wavefunctions which are localized on the vertices.

In table 4, I report the energy (multiplied by h^2) of the bound states and of the first unbound state (E_{gap}) for the different configurations. These results have been obtained using a fine grid corresponding to $h = 1/300$ and show that the bound states are precisely $\bar{n}^2$ as anticipated and they are essentially degenerate; the energy of the bound states and of the gap are also found to be almost insensitive to $\bar{n}$, which can be interpreted as a sign of confinement of a state to the crossings. I have also checked the dependence of these results upon N (or equivalently upon h) observing that the energies can be fitted excellently as $E = a + b/N^2$; for example, in the case of the ground state of the configuration with $\bar{n} = 4$, I have obtained $E = 2.59874 - 44.6364/N^2$.

In figure 14, I have plotted the wavefunction of the ground state of the configuration corresponding to $\bar{n} = 4$ using a grid with $N = 500$. The wavefunction is clearly localized at the crossings between the wires. Similar behaviour is observed for the remaining 15 bound states.

7. Collocation with conformal mapping

The examples considered in the previous sections show that it is possible to obtain the spectrum of the negative Laplacian over regions of arbitrary shape by using a collocation scheme, where the boundary conditions need not to be explicitly enforced on the border. Clearly, the precision of this approach should improve if the boundary conditions would be enforced exactly on the border of the membrane. One way of achieving this result is by mapping conformally the shape of the membrane into a square (or a rectangle), on whose border the LSF obey Dirichlet boundary conditions. I will discuss explicitly two examples of how this is done.

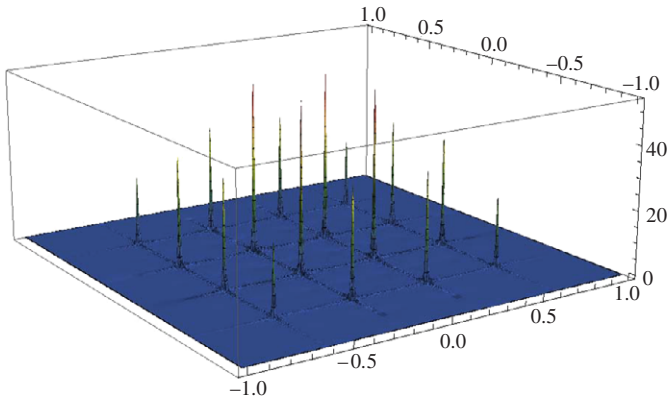

Figure 14. Wavefunction of the ground state of the configuration for $\bar{n} = 4$ using $N = 500$.

Table 4. Energies of the bound states for configurations with different number of crossings, using $N = 600$, corresponding to a spacing $h = 1/300$.

$\bar{n}$	1	2	3	4
h^2E_1	2.59873	2.59871	2.59867	2.59862
h^2E_2	–	2.59873	2.59869	2.59864
h^2E_3	–	2.59873	2.59869	2.59864
h^2E_4	–	2.59876	2.59872	2.59867
h^2E_5	–	–	2.59873	2.59868
h^2E_6	–	–	2.59873	2.59868
h^2E_7	–	–	2.59876	2.59871
h^2E_8	–	–	2.59876	2.59871
h^2E_9	–	–	2.59880	2.59874
h^2E_{10}	–	–	–	2.59874
h^2E_{11}	–	–	–	2.59875
h^2E_{12}	–	–	–	2.59877
h^2E_{13}	–	–	–	2.59877
h^2E_{14}	–	–	–	2.59881
h^2E_{15}	–	–	–	2.59881
h^2E_{16}	–	–	–	2.59887
h^2E_{gap}	3.28997	3.29006	3.29019	3.29035

7.1. Circular membrane

As a first example I consider a circular homogeneous membrane, which is exactly solvable (see, for example [1]) and therefore it can be a useful tool to test the precision of the present method.

The function

$$f(z) = \mathrm{e}^{-\frac{3\mathrm{i}\pi}{4}} \mathrm{sn}\Big(zF\Big(\sin^{-1}\Big(\mathrm{e}^{-\frac{\mathrm{i}\pi}{4}}\Big)\Big| - 1\Big)\Big| - 1\Big) \tag{18}$$

maps the unit square in the w complex plane into the unit circle in the complex z plane, as seen in figure 15. Here, $\mathrm{sn}(a|b)$ is the Jacobi elliptic function sn and $F(a|b)$ is the incomplete elliptic function of first kind.

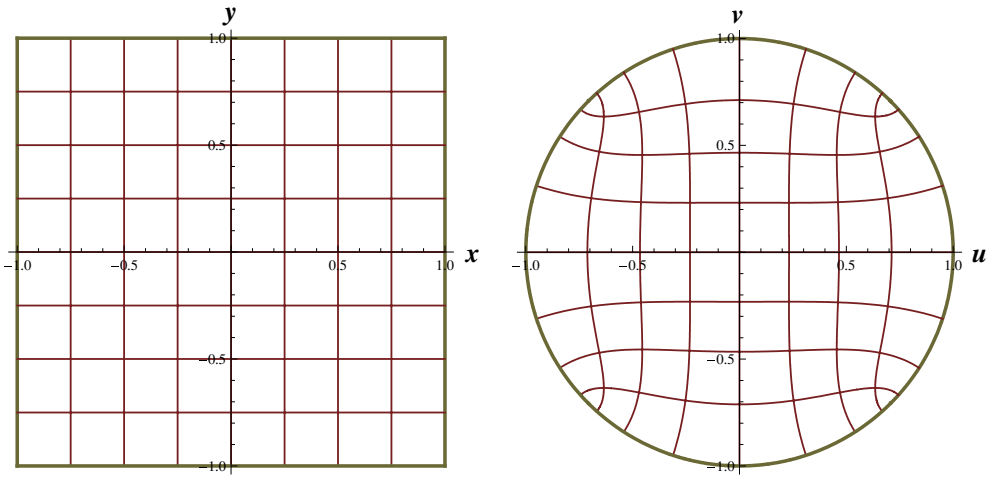

Figure 15. Unit square in the z plane and the corresponding unit circle in the w plane reached through transformation (18).

Under this mapping the original equation,

$$-\Delta\psi(w) = \lambda\psi(w) \tag{19}$$

with Dirichlet boundary conditions on the unit circle, is mapped to

$$-\Delta\chi(z) = \lambda\sigma(z)\chi(z) \tag{20}$$

with Dirichlet boundary conditions on the unit square. Here, $\sigma(z) \equiv \left|\frac{\mathrm{d}w}{\mathrm{d}z}\right|^2$ and equation (20) describes the vibrations of a non-uniform square membrane. Although in the previous sections I have restricted the application of the method to the case of uniform membranes of arbitrary shapes, the method can be applied also to inhomogeneous membranes straightforwardly. Let me briefly mention how this is done. As a first step, equation (20) may be written in the equivalent form

$$-\frac{1}{\sigma(z)}\Delta\chi(z) = \lambda\chi(z). \tag{21}$$

The operator $\hat{O} \equiv \frac{1}{\sigma(z)}\Delta$ is evaluated on a uniform grid in the z-plane using the little sinc functions (LSF). The action of the operator over a product of sinc functions can be calculated very easily, as explained in the previous sections. To make the discussion simpler, I restrict to the equivalent one-dimensional operator and make it act over a single LSF:

$$\begin{aligned} -\frac{1}{\sigma(x)}\frac{\mathrm{d}^2}{\mathrm{d}x^2}s_k(h,N,x) &= -\sum_{jl}\frac{1}{\sigma(x_j)}c^{(2)}_{kl}s_j(h,N,x)s_l(h,N,x) \\ &\approx -\sum_{j}\frac{1}{\sigma(x_j)}c^{(2)}_{kj}s_j(h,N,x). \end{aligned} \tag{22}$$

The matrix representation of the operator over the grid may now be read explicitly from the expression above. The reader should note that the matrix will not be symmetric unless the

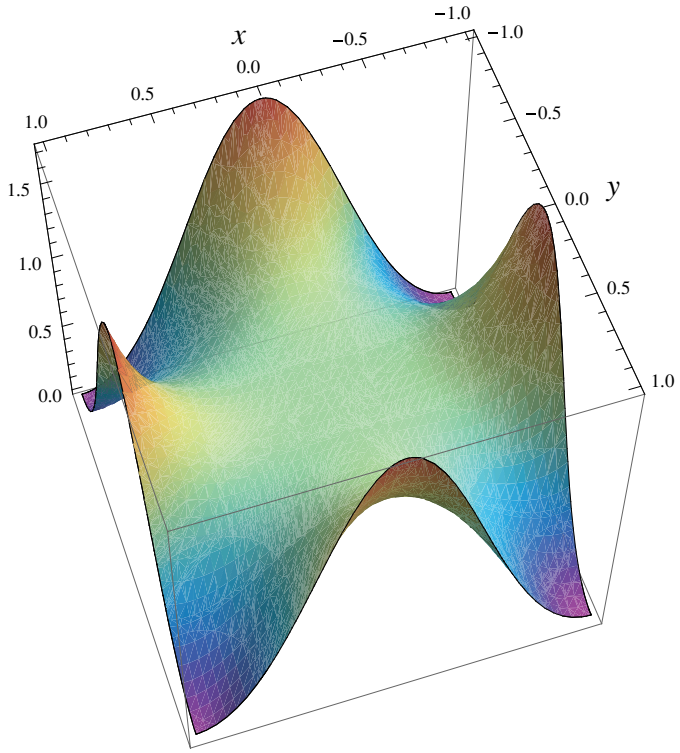

Figure 16. Density of the inhomogeneous square membrane isospectral to the homogeneous circular membrane.

density is constant[3]. Figure 16 displays the density of the inhomogeneous square membrane which is isospectral to the homogeneous circular membrane.

Using this approach I have considered grids with $N = 10, 20, \ldots, 80$ and I have calculated the first four even–even eigenvalues, which are shown in table 5. Taking into account the symmetry of problem I have used symmetrized LSF, which obey mixed boundary conditions (Dirichlet at one end and Neumann at the other end): in this way, for a given value of N a grid of $(N/2)^2$ points is used. As mentioned before the exact eigenvalues for this problem are known (the zeros of the Bessel functions): these are reported in the last row.

In figure 17, I have plotted the lowest eigenvalue of the circular membrane corresponding to different N and I have fitted these points using functions like $c_0 + c_1/N^r$, with $r = 3, 4, 5$ (the dashed, solid and dotted lines, respectively, in the plot). This plot shows that the leading (non-constant) behaviour of the numerical energy for $N \gg 1$ is $1/N^4$.

Taking into account this behaviour, I have considered the quantity

$$\Xi_Q \equiv \sum_{k=1}^{8} \left[\alpha_1 - \sum_{n=2}^{Q} \frac{\alpha_n}{(10k)^{n+2}} \right]^2, \tag{23}$$

where $Q = 8$ and I have obtained the coefficients α_n by minimizing Ξ_Q (note that this expression takes into account the leading $1/N^4$ behaviour just discussed). The row marked as LSQ_8 displays the quite precise results obtained following this procedure.

[3] In general, the calculation of the eigenvalues and eigenvectors of non-symmetric matrices is computationally more demanding than for symmetric matrices of equal dimension.

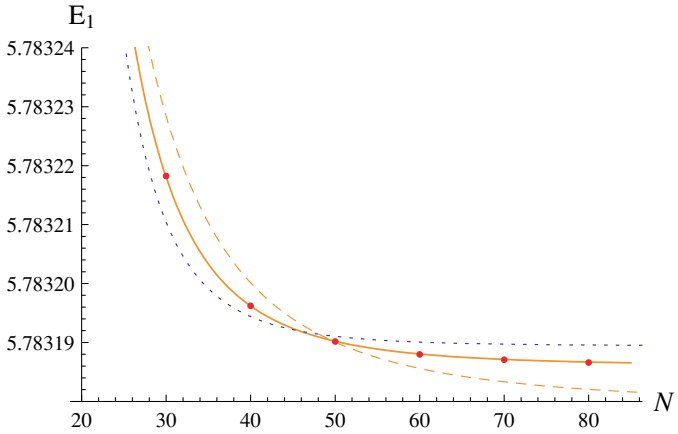

Figure 17. Energy of the ground state of the circular membrane. The dashed, solid and dotted lines correspond to fits using functions like $c_0 + c_1/N^r$, with $r = 3, 4, 5$, respectively.

Table 5. Even–even spectrum of the circular membrane: first four eigenvalues.

N	E_1	E_2	E_3	E_4
10	5.785633618	26.46056162	30.55061880	57.88187288
20	5.783347847	26.37986506	30.47598468	57.60026669
30	5.783218252	26.37564237	30.47217988	57.58626207
40	5.783196213	26.37493961	30.47155075	57.58397911
50	5.783190167	26.37474851	30.47138009	57.58336363
60	5.783187992	26.37468004	30.47131902	57.58314408
70	5.783187059	26.37465074	30.47129291	57.58305035
80	5.783186606	26.37463653	30.47128023	57.58300497
LSQ_8	5.783185971	26.37461646	30.47126209	57.58294087
Exact	5.783185962	26.37461642	30.47126234	57.58294090

I would like to discuss briefly a different issue. In [34], Gottlieb has used the Moebius transformation

$$f_g(z) = (z - a)/(1 - az) \tag{24}$$

to map the unit circle onto itself. This mapping transforms the homogeneous Helmholtz equation for a circular membrane into the inhomogeneous Helmholtz equation for a circular membrane with density

$$\rho(x, y) = |f_g'(z)|^2 = \rho_0 \frac{(1 - a)^2}{[(1 - ax)^2 + a^2 y^2]^2}. \tag{25}$$

Gottlieb uses this result to conclude that membranes corresponding to different densities, i.e. different values of a, are isospectral, thus providing a negative answer to the famous question 'Can one hear the shape of a drum?', posed by Kac [16]. I wish to move our discussion on computational grounds: for a given a the mapping of equation (24) deforms the grid inside the unit circle; as a is changed, the grid points move, as shown in figure 18. The case $a = 0$ is plotted in the right panel of figure 15. Clearly, if the density of the membrane is constant, or symmetric with respect to the centre, one expects that $a = 0$ provide the best grid. In figure 19, I have plotted the logarithm of the difference between the approximate

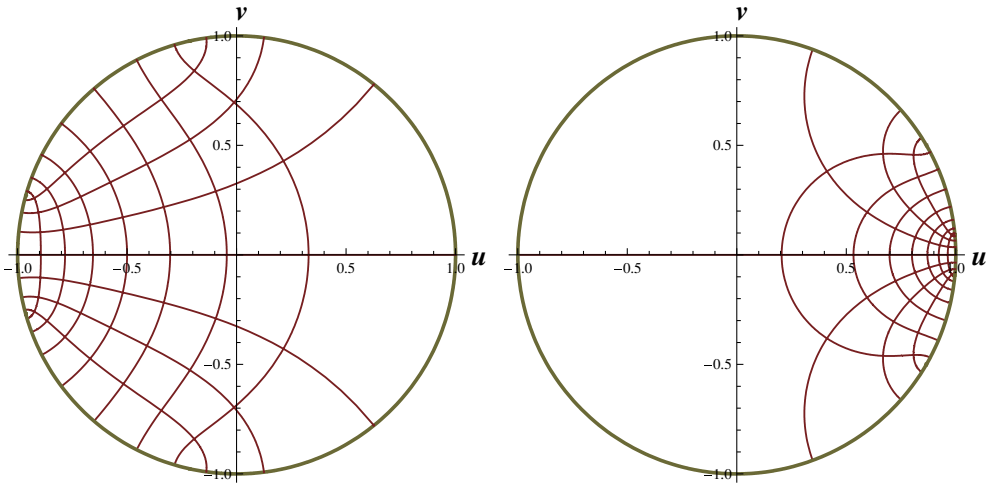

Figure 18. Grid obtained with the Moebius map corresponding to $a = 0.5$ (left) and $a = -0.8$ (right).

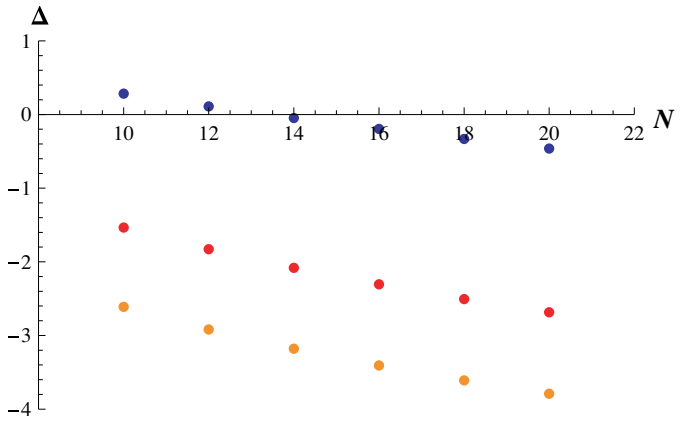

Figure 19. $\Delta \equiv Log_{10}(E_N - E_{\text{exact}})$ using three values of a ($a = 0, 0.4$ and 0.8 from bottom to top).

and exact energy for the ground state of a circular membrane, $\Delta \equiv Log_{10}(E_N - E_{\text{exact}})$, using three values of a ($a = 0, 0.4$ and 0.8). These numerical results confirm the prediction made: stated in different terms one can conclude that *for a given problem one can improve the numerical accuracy of a calculation by selecting an optimal grid among those obtained through a conformal map of the region onto itself.* The optimization of the parameter a depending on the specific problem considered is in the same spirit of the variational approach used in [13, 14, 35] and could provide a useful computational tool to boost the precision of the results.

7.2. Circular waveguide

The second example of the application of conformal mapping to the solution of the Helmholtz equation is taken from the paper of Kuttler and Sigillito [2] (this problem was also studied earlier by Moler, in [101] of [2]).

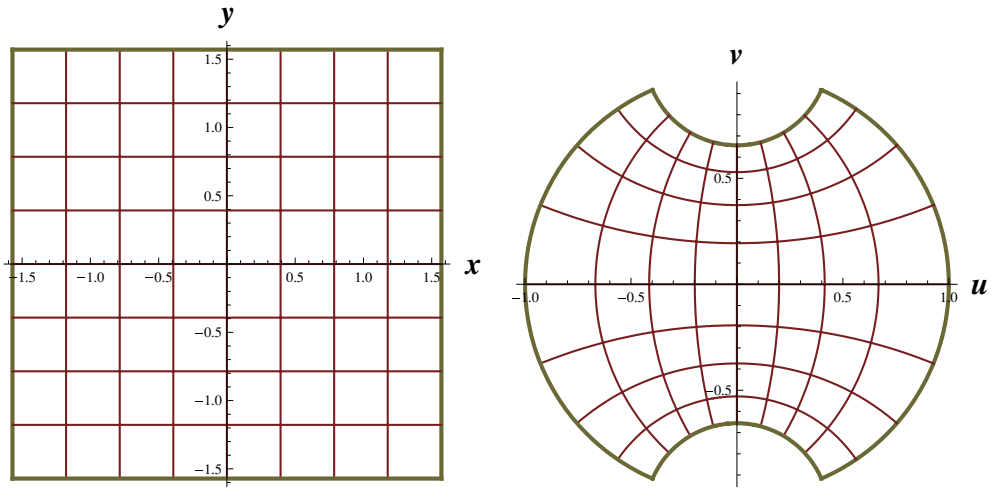

Figure 20. Square in the z plane and corresponding region in the w plane, reached through the conformal map $w = \tan\frac{z}{2}$.

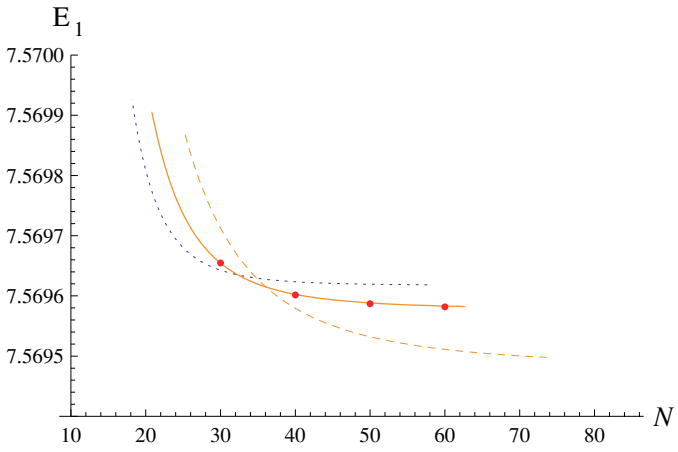

Figure 21. Energy of the ground state of the circular waveguide. The dashed, solid and dotted lines correspond to fits using functions like $c_0 + c_1/N^r$, with $r = 3, 4, 5$, respectively.

In figure 20, two regions of the plane are displayed: the left plot corresponds to a square of side π centred on the origin in the $z = x + \mathrm{i}y$ plane; the right plot corresponds to a circular waveguide with circular ridges in the $w = u + \mathrm{i}v$ plane. The function $w = \tan\frac{z}{2}$ maps the first region into the second one.

As I have shown for the case of the circular membrane, the homogeneous Helmholtz equation over the second region may be transformed into an inhomogeneous Helmholtz equation over the square:

$$-\Delta U(z) = \lambda\sigma(z)U(z). \tag{26}$$

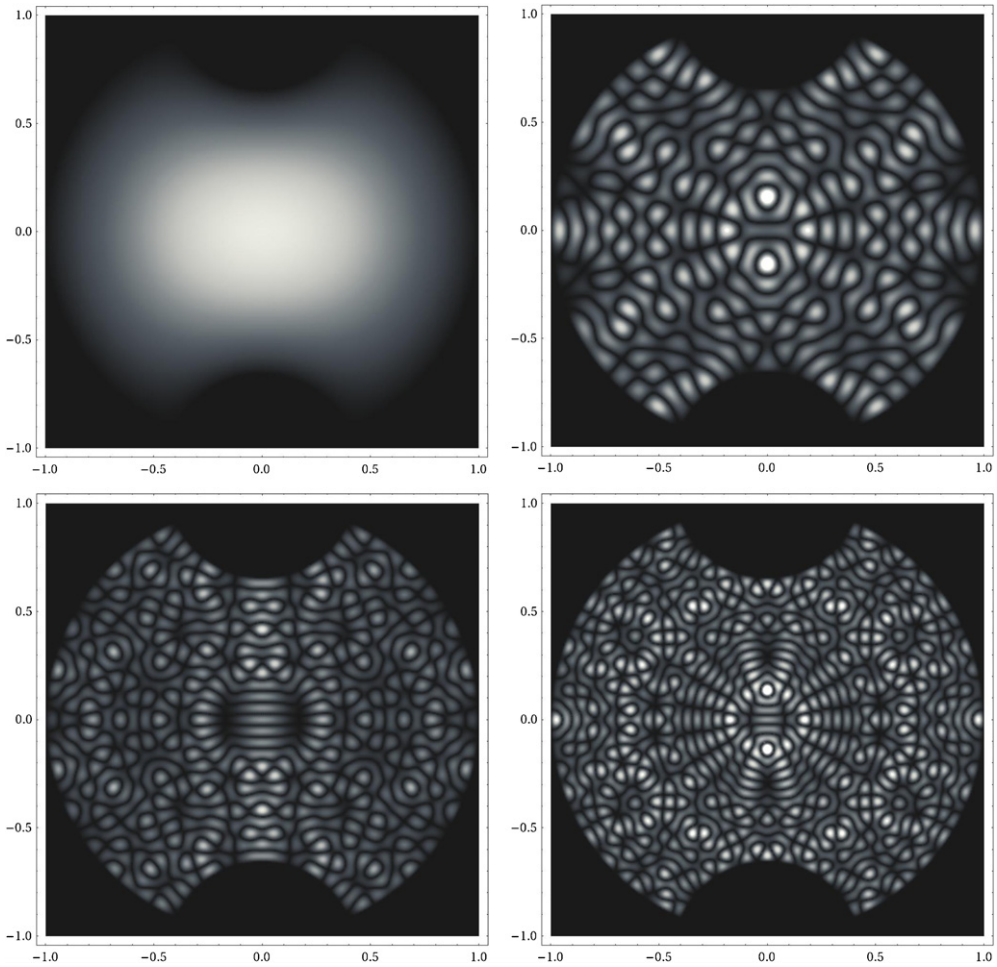

Figure 22. Upper panel: Even–even wavefunctions (absolute value): ground state and 100th excited state of the circular waveguide. Lower panel: Even–even wavefunctions (absolute value): 200th and 300th excited states of the circular waveguide. A grid with $N = 80$ is used.

In the present case $\sigma(z) \equiv \left|\frac{dw}{dz}\right|^2 = (\cos x + \cosh y)^2$, and Dirichlet boundary conditions are assumed on the borders of the two regions.

In tables 1–3 of their paper, Kuttler and Sigillito report different estimates for the first 12 even–even eigenvalues, obtained using different approaches. In table 2 they also apply Richardson extrapolation to the eigenvalues obtained with finite difference. In the case of the ground state of this membrane they also mention the precise value obtained by Moler using the method of point matching

$$\lambda_1 = 7.5695769, \tag{27}$$

In table 6, I report the even–even eigenvalues of equation (26) obtained using collocation with different values of N. The results corresponding to the ground state are plotted in figure 21 and fitted using functions like $c_0 + c_1/N^r$, with $r = 3, 4, 5$ (the dashed, solid

Table 6. Even–even eigenvalues of the problem of equation (26) using collocation with the little sinc functions (LSF).

N	E_1	E_2	E_3	E_4
10	7.575738906	29.35369905	44.93667650	68.99532514
20	7.569970385	29.12882337	44.84592568	67.91298030
30	7.569654735	29.11799633	44.84124500	67.86357065
40	7.569601533	29.11623444	44.84047707	67.85592485
50	7.569586991	29.11575957	44.84026961	67.85390710
60	7.569581767	29.11559019	44.84019553	67.85319500
70	7.569579528	29.11551787	44.84016389	67.85289283
80	7.569578441	29.11548286	44.84014857	67.85274711
LSQ_8	7.569576902	29.11543343	44.84012692	67.85254236
LSQ_7	7.569576902	29.11543343	44.84012692	67.85254236
N	E_5	E_6	E_7	E_8
10	76.36327173	105.8649443	127.5818229	147.6128111
20	74.57343676	104.7105731	123.4501146	137.5136748
30	74.51254455	104.6448241	123.2916952	137.1508752
40	74.50340797	104.6345417	123.2690972	137.1033030
50	74.50101871	104.6318226	123.2633192	137.0914797
60	74.50017885	104.6308625	123.2613110	137.0874237
70	74.49982321	104.6304550	123.2604661	137.0857295
80	74.49965192	104.6302584	123.2600608	137.0849203
LSQ_8	74.49941161	104.6299823	123.2594952	137.0837970
LSQ_7	74.49941160	104.6299823	123.2594952	137.0837959
N	E_9	E_{10}	E_{11}	E_{12}
10	152.6380731	175.0500571	202.7827432	229.6150278
20	147.1852075	177.5293898	193.4167694	213.4362048
30	147.1167888	177.2332164	193.0075863	212.8440230
40	147.1064916	177.1901085	192.9541314	212.7718374
50	147.1038082	177.1790645	192.9409198	212.7546507
60	147.1028673	177.1752263	192.9364009	212.7488774
70	147.1024696	177.1736121	192.9345164	212.7464938
80	147.1022783	177.1728379	192.9336173	212.7453635
LSQ_8	147.1020103	177.1717582	192.9323707	212.7438068
LSQ_7	147.1020110	177.1717573	192.9323707	212.7438134

and dotted lines, respectively, in the plot). This plot proves that the leading (non-constant) behaviour of the numerical energy for $N \gg 1$ is $1/N^4$, as for the circular membrane.

The results in the table have also been extrapolated using a least square approach

$$\Xi_Q \equiv \sum_{k=1}^{8} \left[\alpha_1 - \sum_{n=2}^{Q} \frac{\alpha_n}{(10k)^{n+2}} \right]^2, \tag{28}$$

where $Q = 7, 8$ and α_n are coefficients which are obtained by minimizing Ξ_Q. Note that this expression takes into account the leading $1/N^4$ behaviour just discussed. The rows marked as $LSQ_{7,8}$ display the results obtained following this procedure (the comparison between the results for $Q = 7$ and $Q = 8$ gives an indication over the precision reached): in particular, the energy of the ground state reproduces all the digits of the result obtained by Moler. It is also remarkable that the energies obtained with the conformal-collocation method decrease

monotonically when the number of collocation points is increased (the only exception is represented by the E_{10} for $N = 10$, probably due to the limited number of collocation points).

As a technical remark, one should note that the results corresponding to a given value of N are obtained using a set of $N/2$ symmetric (even) functions for each direction, thus reducing the computation load by a factor of 4. The results displayed in this table should be compared with the analogous results of table 2 of [2], which were obtained using finite difference. Four different wavefunctions of the circular waveguide, corresponding to the ground, 100th, 200th and 300th even–even excited states are shown in figure 22.

8. Conclusions

In this paper, I have used a collocation method based on LSF to obtain the numerical solutions of the Helmholtz equation over two-dimensional regions of arbitrary shape. A large number of examples have been studied, illustrating the great potentialities of the present method. Among the principal virtues of this method I would like to mention its generality (it can be applied to membranes of arbitrary shapes, including inhomogeneous membranes, and to the Schrödinger equation—although I have not done this in the present paper), its simplicity (the matrix representation of the Helmholtz operator is obtained directly by collocation, and therefore it does not require the calculation of integrals) and the possibility of combining it with a conformal mapping, as done in the last section. In this last case, a rapid convergence to the exact eigenvalues is observed as the number of grid points is increased. In the case where the border is not treated exactly, it has also been observed that the method provides monotonous sequences of approximations to the exact eigenvalue either from above or from below. Readers interested to looking at more examples of application of this method may find useful to check the gallery of images which can be found at http://fejer.ucol.mx/paolo/drum.

Appendix. Mesh refinement

Although the collocation method described in this paper allows one to obtain precise solutions to the Helmholtz equation over domains of arbitrary shape, in general the Dirichlet boundary conditions are not enforced exactly over all the boundary. As discussed in section 7, the best approach consists of introducing a conformal map, which allows one to go from the original problem to an inhomogeneous Helmholtz problem over a square: in such a case, the Dirichlet boundary conditions are imposed exactly and rapid convergence to the exact solutions is observed. In general, however, finding such a conformal map can be a difficult task and therefore the first approach may be more appealing. I will discuss here a simple procedure to 'refine' the results obtained by direct collocation of the Helmholtz equation over the grid. The fundamental observation is that the LSF that we have used do vanish on the grid points on the border and external to the membrane, but they are nonzero in all the other points external to the membrane. Therefore, the cumulative effects of the LSF internal to the membrane can be seen also outside the membrane, although it will tend to disappear as the number of grid points is increased. This solution, to increase the number of grid points, may be the most obvious but is certainly not appealing computationally, since increasing the number of grid points strongly increases the computational cost (remember that the number of matrix elements grows as N^4). However, we can use much simpler procedure, which does not require any additional diagonalization. Call N the parameter defining the size of the grid:

a point in this grid is described by the direct product of the LSF in the x and y directions. In the Dirac notation, we write

$$\langle x, y|k, k'\rangle_h \approx s_k(h, x)s_{k'}(h, y), \tag{A.1}$$

assuming for simplicity that the grid has the same spacing in both directions. Let us now concentrate on one of the LSF, say the one in the x direction: we take a finer grid, with a spacing $h' = h/l$, where l is an integer. The new grid contains now $(lN - 1)$ points, including obviously the original grid points. However, it is clear that the original LSF can be decomposed in the new grid as

$$s_k(h, x) = \sum_{j=-lN/2+1}^{lN/2-1} s_k(h, \bar{x}_j)s_j(h/l, x), \tag{A.2}$$

where $\bar{x}_j = 2Lj/(lN)$ are the new grid points. Note that this relation is exact.

The wavefunction of the nth state obtained from the diagonalization of the $(N-1)\times(N-1)$ Hamiltonian reads

$$\begin{aligned}\psi_n(x, y) &= \frac{1}{h}\sum_K v_K^{(n)} s_{k(K)}(h, x)s_{k'(K)}(h, y)\\ &= \frac{1}{h}\sum_K v_K^{(n)} \sum_{j=-lN/2+1}^{lN/2-1} s_{k(K)}(h, \bar{x}_j)s_j(h/l, x) \sum_{j'=-lN/2+1}^{lN/2-1} s_{k'(K)}(h, \bar{y}_{j'})s_{j'}(h/l, y),\end{aligned}$$

where $v^{(n)}$ is the nth eigenvector. Clearly, $\psi_n(x, y)$ differs from 0 even in points of the refined grid which fall outside the membrane profile. We introduce a new matrix whose elements are given by

$$\eta_{jj'} = \begin{cases} 0 & \text{if } (\bar{x}_j, \bar{y}_{j'}) \notin \mathcal{B} \\ 1 & \text{if } (\bar{x}_j, \bar{y}_{j'}) \in \mathcal{B} \end{cases} \tag{A.3}$$

and rewrite the wavefunction 'purged' on the refined grid as

$$\bar{\psi}_n(x, y) = \frac{\mathcal{N}}{h} \sum_{j=-lN/2+1}^{lN/2-1} \sum_{j'=-lN/2+1}^{lN/2-1} \tilde{V}_{jj'}s_j(h/l, x)s_{j'}(h/l, y),$$

where

$$\tilde{V}_{jj'} \equiv \eta_{jj'} \sum_K v_K^{(n)} s_{k(K)}(h, \bar{x}_j)s_{k'(K)}(h, \bar{y}_{j'}) \tag{A.4}$$

and $\mathcal{N}$ is a normalization constant that ensures that

$$\int_{\mathcal{B}} \psi_n^2(x, y)\, \mathrm{d}x\, \mathrm{d}y = 1. \tag{A.5}$$

It is easy to show that

$$\mathcal{N} = \frac{l}{\sqrt{\sum_{jj'} \tilde{V}_{jj'}^2}}. \tag{A.6}$$

To simplify the notation, I define

$$\mathcal{V}_{jj'} \equiv \frac{\mathcal{N}}{l}\tilde{V}_{jj'} \tag{A.7}$$

and thus write

$$\bar{\psi}_n(x, y) = \frac{l}{h} \sum_{j=-lN/2+1}^{lN/2-1} \sum_{j'=-lN/2+1}^{lN/2-1} \mathcal{V}_{jj'}s_j(h/l, x)s_{j'}(h/l, y).$$

On the other hand, we may also calculate the expectation value of the Hamiltonian in this state

$$\begin{aligned}\langle \hat{H} \rangle_n &= -\int_{\mathcal{B}} \bar{\psi}_n(x, y) \Delta \bar{\psi}_n(x, y)\, \mathrm{d}x\, \mathrm{d}y \\ &= -\sum_{jj'rr'ss'} \frac{\mathcal{V}_{jj'}\mathcal{V}_{rr'}}{h^2}\left[\bar{c}^{(2)}_{rs}\delta_{r's'} + \bar{c}^{(2)}_{r's'}\delta_{rs}\right] \int_{\mathcal{B}} s_j(h/l, x) s_{j'}(h/l, y) s_s(h/l, x) s_{s'}(h/l, y) \\ &= -\sum_{jj'rr'} \mathcal{V}_{jj'}\mathcal{V}_{rr'}\left[\bar{c}^{(2)}_{rj}\delta_{r'j'} + \bar{c}^{(2)}_{r'j'}\delta_{rj}\right] \\ &= -\sum_{jj'r} \bar{c}^{(2)}_{rj}[\mathcal{V}_{jj'}\mathcal{V}_{rj'} + \mathcal{V}_{j'j}\mathcal{V}_{j'r}], \end{aligned} \tag{A.8}$$

where $\bar{c}^{(2)}$ is the matrix for the second derivative on the refined grid. An example of application of this procedure is shown in figure 13.

References

[1] Fetter A L and Walecka J D 1980 *Theoretical Mechanics of Particles and Continua* (New York: McGraw Hill)
[2] Kuttler J R and Sigillito V G 1984 Eigenvalues of the Laplacian in two dimensions *SIAM Rev.* **26** 163–93
[3] Reid J K and Walsh J E 1965 An elliptic eigenvalue problem for a reentrant region *J. Soc. Indust. Appl. Math.* **13** 837–50
[4] Fox L, Henrici P and Moler C B 1967 Approximations and bounds for eigenvalues of elliptic operators *SIAM J. Numer. Anal.* **4** 89–102
[5] Mason J C 1967 Chebyshev polynomial approximations for the L-membrane eigenvalue problem *SIAM J. Appl. Math.* **15** 172
[6] Milsted M C and Hutchinson J R 1974 Use of trigonometric terms in the finite element method with application to vibrating membranes *J. Sound Vib.* **32** 327–46
[7] Sideridis A B 1984 A numerical solution of the membrane eigenvalue problem *Computing* **32** 167–76
[8] Schiff B 1988 Finite element eigenvalues for the Laplacian over an L-shaped domain *J. Comput. Phys.* **76** 233–42
[9] Platte R B and Driscoll T A 2004 Computing eigenmodes of elliptic operators using radial basis functions *Comput. Math. Appl.* **48** 561–76
[10] Betcke T and Trefethen L N 2005 Reviving the method of particular solutions *SIAM Rev.* **47** 469–91
[11] Trefethen L N and Betcke T 2006 Computed eigenmodes of planar regions *AMS Contemp. Math.* **412** 297–314
[12] Kaufman D L, Kosztin I and Schulten K 1999 Expansion method for stationary states of quantum billiards *Am. J. Phys.* **67** 133–41
[13] Amore P, Cervantes M and Fernández F M 2007 Variational collocation on finite intervals *J. Phys. A: Math. Theor.* **40** 13047–62
[14] Amore P 2007 Alternative representation of nonlocal operators and path integrals *Phys. Rev.* A **75** 032111
[15] Berry M V 1987 Improved eigenvalues sums for inferring quantum billiards *J. Phys. A: Math. Gen.* **20** 2389–403
[16] Kac M 1966 Can one hear the shape of a drum? *Am. Math. Mon.* **73** 1–23
[17] Gordon C, Webb D and Wolpert S 1992 Isospectral plane domains and surfaces via Riemannian orbifolds *Invent. Math.* **110** 1–22
[18] Sridhar S and Kudrolli L 1994 Experiments on not 'hearing the shape' of drums *Phys. Rev. Lett.* **72** 2175–8
[19] Dhar A, Rao D M, Shankar U and Sridhar S 2003 Isospectrality in chaotic billiards *Phys. Rev.* E **68** 026208
[20] Wu H, Sprung D W L and Martorell J 1995 Numerical investigation of isospectral cavities built from triangles *Phys. Rev.* E **51** 703–8
[21] Driscoll T A 1997 Eigenmodes of isospectral drums *SIAM Rev.* **39** 1–17
[22] Bender C M and Orszag S A 1978 *Advanced Mathematical Methods for Scientists and Engineers* (New York: McGraw Hill)
[23] Trott M 2005 The sound of an unusual drum *Math. J.* **9** (3)
[24] Sapoval B, Gobron T and Margolina A 1991 Vibrations of fractal drums *Phys. Rev. Lett.* **67** 2974–8
[25] Haeberlé O, Sapoval B, Menou K and Vach H 1998 Observation of vibrational modes of irregular drums *Appl. Phys. Lett.* **73** 3357–9

[26] Even C, Russ S, Repain V, Pieranski P and Sapoval B 1999 Localization in fractal drums: an experimental study *Phys. Rev. Lett.* **83** 726–9
[27] Hobiki Y, Yakubo K and Nakayama T 1995 Spectral distribution of drums with fractal perimeters: the Weyl–Berry–Lapidus conjecture *Phys. Rev.* E **52** R1310–2
[28] Neuberger J M, Sieben N and Swift J W 2006 Computing eigenfunctions on the Koch snowflake: a new grid and symmetry *J. Comput. Appl. Math.* **191** 126–42
[29] Banjai L 2007 Eigenfrequencies of fractal drums *J. Comput. Appl. Math.* **198** 1–18
[30] Schult R L, Ravenhall D G and Wyld H W 1989 Quantum bound states in a classically unbound system of crossed wires *Phys. Rev.* B **39** 5476–9
[31] Avishai Y, Bessis D, Giraud B G and Mantica G 1991 Quantum bound states in open geometries *Phys. Rev.* B **44** 8028–34
[32] Levin D 2004 On the spectrum of the Dirichlet Laplacian on broken strips *J. Phys. A: Math. Gen.* **37** L9–11
[33] Goldstone J and Jaffe R L 1992 Bound states in twisting tubes *Phys. Rev.* B **45** 14100–7
[34] Gottlieb H P W 1988 Density distribution for isospectral circular membranes *SIAM J. Appl. Math.* **48** 948–51
[35] Amore P 2006 A variational sinc collocation method for strong-coupling problems *J. Phys.* A **39** L349–55